JOURNAL OF THEORETICAL AND APPLIED MECHANICS
48, 2, pp. 479-504, Warsaw 2010

FOURIER EXPANSION SOLUTION FOR A SWITCHED SHUNT CONTROL APPLIED TO A DUCT

Salvatore Ameduri

The Italian Aerospace Research Centre, Capua, Italy

e-mail: s.ameduri@cira.it

Monica Ciminello

"Federico II" University of Naples, Aerospace Engineering Department, Naples, Italy

e-mail: monica.ciminello@gmail.com

In the present work, a semi analytic approach aimed at estimating the effects on reduction of the pressure sound level by synchronised switched shunt logic is described. The displacement field within a 1D longitudinal air column through a Fourier series expansion has been formalised by assigning a sinusoidal perturbation and fluid-structure interface condition on the left and right boundaries, respectively. To simulate the no control operative condition, the solution has been computed for the entire time domain, keeping invariant all circuitry properties; then for the switch working modality, the solution has been computed by splitting the entire time domain into partitions; for any partition, specific circuitry properties (e.g. piezo voltage, electrical field...) have been selected. Based on the displacement information, the related sound pressure level has been compared for no controlled and controlled operative conditions, with and without signal amplification.

Key words: synchronised switched shunt control, piezoelectric, pressure sound level

Nomenclature

T_{el}, T_{mech} – electrical circuit and mechanical period, respectively
T_{tot} – total simulation time
t_0 – initial instant
x, y, z – axis, fluid column length, depth and height, respectively
U_0 – excitation amplitude

$u_0(t)$ – displacement at $x = 0$

$p(x,t)$ – pressure

ω – excitation angular frequency

c – sound speed

ξ – fluid decay rate

L – fluid column length

M_p – piezo transmitted moment

d – half beam span

b – depth of the column and of the beam

ζ – piezo extension along the beam span, $\zeta \in [0,1]$

D – bending stiffness

ρ – fluid density

E_0 – boundary conditions constant term

β_1, β_2 – boundary conditions coefficient, proportional to velocity and displacement, respectively

$f(x), g(x)$ – initial displacement and initial velocity law, respectively

$v(x,t)$ – function used for boundary conditions homogenisation

$u(x,t)$ – semi-analytic solution, displacement distribution

$P(x,t)$ – differential equation right hand term of the boundary conditions homegeneous problem

$Q(x,t), R(x,t)$ – displacement and velocity initial conditions right hand term of the boundary conditions homegeneous problem, respectively

$X(x), T(t)$ – space and time depending factor of the solution, respectively

λ_n – n-th problem eigen value

$\varphi_n(x), b_n(t)$ – n-th orthogonal space and n-th time dependent function used for Fourier series expansion, respectively

$p_n(t), q_n(t)$ – n-th coefficient of Fourier series expansion of $P(x,t)$ and $Q(x,t)$, respectively

D_{1n}, D_{2n} – n-th general integral constants

A_n, B_n – n-th particular integral constants

$\mu_n, \nu_n, r_n(t)$ – n-th coefficient of Fourier series expansion of $f(x)$, $g(x)$ and $R(x,t)$, respectively

$\widehat{p}$ – pressure squared value, averaged with respect time and space

d_{31}, g_{31} – piezoelectric charge and voltage constant, respectively

Y_p, Y_s – piezoelectric and structure Young modulus, respectively

ν_p, ν_s – piezoelectric and structure Poisson modulus, respectively

1. Introduction

Sound and vibration control can be considered a real technological challenge because of the large amount of related problems and peculiar complexity. As a consequence, many efforts have been spent on defining, realising and characterising different typologies of control techniques, tailored on the specific problem.

Among the different strategies, due to their promising properties in terms of lightness, simple design and low cost, a wide amount of interest has been focused on the shunt circuits. Through the shunt control architectures, structural vibrations are reduced by using time variant electric circuits integrated with electromechanical PZT suitably positioned on structural elements.

The first three schemes illustrated on the left in Fig. 1 represent the most common passive shunt circuits. A lot of works in literature (Erturk and Inman, 2008; Hagood and Von Flotow, 1991; Lesieutre, 1998; Park and Inman, 1999) have shown how the resistive shunt dissipates energy through Joule effect, the capacitive shunt changes the local stiffness of the structure, while shunting with inductive introduces an electrical resonance, which can be optimally tuned to the one of the system, analogously with a mechanical vibration absorber.

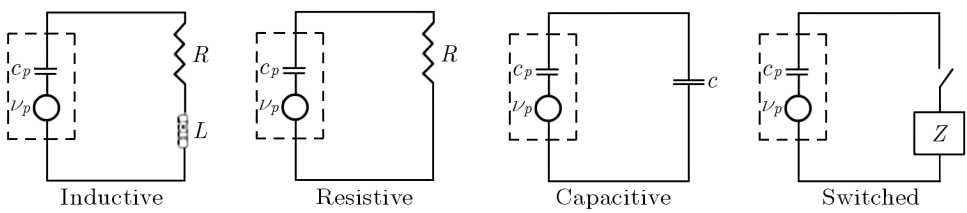

Fig. 1. Configuration of four different shunted circuits

It is well known that passive techniques are among the most commonly adopted because they never provide the structure with artificial energy and their functionality is essentially based on time invariant (fixed) modifications of the structural mass, damping and stiffness matrices. However, despite their easy implementation and low cost, their performance is generally inadequate to face all the necessities, particularly concerned with optimal strategies of smart structures solutions. In this case in fact, the control system characteristics have to satisfy some important requirements, among all, adaptability of the parameters.

This is the reason why in recent years there has been a growing interest in the semi-active control. A semi-active device can be broadly defined as a passive device in which the properties (stiffness, damping, etc.) can be varied in real time with a low power input. Although they behave in a strongly

nonlinear way, semi-active devices are inherently passive and cannot destabilise the system. They are also less vulnerable to power failure and have good thermal stability, particularly useful in aerospace applications (De Marneffe *et al.*, 2008; Preumont, 1997). These reasons, jointly with the good performance exhibited within the low frequency range, justified the large amount of theoretical, numerical and experimental investigations. Among the shunt schemes sketched in Fig. 1, the last on the right represents the switch architecture. The principle of the shunt using a switch is to store the electric charge and use its effect in opposition to the structural movement within a very short time constant.

One of the first concepts of commutation of a shunted circuit was proposed in Clark (1999, 2000), where the author studied a case of resistive shunt with comparable open and closed circuit periods (this is the reason why it is referred as "state switching"). This kind of system can be assimilated to a variable stiffness mechanical system.

In Richard *et al.* (1999, 2000), the authors proposed to close the circuit for a very short period and to add an inductor to augment the charge on the PZT device. This technique is called "Synchronized Switch Damping", that can be specialised according to the following shunt architecture:

- Synchronized Switch Damping on Short, where the shunt is purely resistive;
- Synchronized Switch Damping on Inductance, with an inductive component;
- Synchronized Switch Damping on Voltage source, where the shunt includes a voltage source (Lefeuvre *et al.*, 2006)] (which place the system in the class of the active control, needing an external power supply) and involves a risk of instability. This problem can be mitigated with a slow variation of the voltage following the average amplitude of the vibrations, as proposed in Lallart *et al.* (2005).

In the cited works dealing with this technique, the damping was estimated with a simple 1D model. The development and implementation of mdof models have also been faced.

The team of Clark (Corr and Clark, 2001, 2002; Corr, 2001) compared the state switching and the synchronised switching showing that the last one is more effective. Further improvements were presented in Corr and Clark (2003) where the authors developed the switching synchronisation technique based on different modal filters. The technique required complex filters and power supply, but the performance was good. This kind of work is at the moment an object of another American staff (Collinger and Wickert, 2007).

The team of Daniel Guyomar refined the inductive switched shunt and proposed an autonomous circuit (Petit *et al.*, 2002, 2004). They showed that the detection of a local maximum is not optimal for the case of multimodal control. The authors proposed probabilistic criteria (detection of maxima significantly exceeding the average level) giving a good result (Guyomar and Badel, 2006).

The necessity of extending benefits due to this technique to more realistic applications has led to numerical solving schemes, prevalently based on a FE approach. Some test cases have been carried out, including this time some examples also on elasto-acoustic systems.

In their works, Ameduri, Ciminello *et al.* (2008a-c) studied the finite element formulation of a synchronised switched shunt applied to both isotropic and anisotropic structure with collocated PZT patches. The multimodal control was optimised by a genetic algorithm. Finally, an original circuit based on a tachometer component was presented.

However, due to the complexity of real applications, despite the efficient reduction techniques employed, numerical computations result heavy and, consequently, time consuming. On the contrary, a semi-analytical solution would allow eliminating the time consumption due to the integration.

In his work, Ameduri *et al.* (2007) faced with the implementation of a semi-analytical solution of a however complex structural system suitably reduced. Then, the analytical solution to the related system of differential equations, for a sinusoidal and constant excitation, was found out; finally, the theoretical solution was fitted to the specific problem, i.e. the switch shunt control implementation.

In Ducarne *et al.* (2007), a multi degree-of-freedom (dof) electromechanical model of a structure with piezoelectric elements coupled to state switching and synchronous switching electric circuits was derived. By restricting the analysis to one mechanical dof only, the system free response was analytically obtained. A similar analysis was conducted to obtain the forced response of the structure subjected to harmonic forcing of any frequency, except that no analytical expressions were available. As a general conclusion, it was proved that the only parameter that influences the performances of the synchronous switching devices was the coupling coefficient, that had to be maximised in order to enhance the vibration attenuation.

The interest in extending switched shunt control benefits also to acoustic applications is confirmed by the amount of numerical and experimental investigations carried out as regards (Ducarne *et al.*, 2007; Guyomar and badel, 2006; Petit *et al.*, 2002). These works deal with the problem of controlling

the sound transmission properties of structural elements used to insulate an internal noise source from the external environment. Another problem is the sound pressure level attenuation within enclosures. The fundamental idea is to implement a control acting on a PZT network, suitably distributed on the boundary of the enclosure (Ciminello *et al.*, 2008b). The effects originated from this solution can be appreciated by predicting and/or measuring the sound pressure level at different points of the air volume taken into consideration.

In the work at hand, the attention is paid to this last problem: pressure sound level attenuation through a switched shunt architecture implemented on a metallic plate, acting on a finite length air column. A semi-analytical approach, consisting in solving the telegraph equation through the Fourier expansion series strategy, has been adopted to find out the time dependent displacement field along the 1D horizontal air column. The related boundary conditions have been assigned by imposing a sinusoidal perturbation on the left frontier and by formalising the fluid-structure interaction on the right side. Here, a couple of PZT patches bonded on the two faces of an aluminium plate and connected to an external switched shunt circuit, provide the control action on the air column.

Before computing the solution, a preliminary validation process has been carried out by verifying the satisfaction of the assigned conditions and proving its convergence by estimating the series coefficients.

Then the simulation of the displacement field within the fluid domain, in presence and absence of control, at different amplification levels, has been performed. For the no control condition, the solution has been computed within the considered time interval; on the other hand, due to the non-linearity of the switch architecture, the controlled solution has been estimated at a different time interval: any partition is limited by the instants at which the circuit is switched on and electrical properties (i.e. voltage, electrical field, charge on the leads) undergo variation.

The results have been expressed in terms of the displacement and sound pressure level computed in different points of the spatial domain; finally, the global attenuation achieved has been evaluated by squared average values of the sound pressure level over spatial and time domains.

2. Switched shunt control system

The adopted electrical network is an RLC resonant circuit having the PZT as capacitor. In Fig. 2, the circuit is sketched.

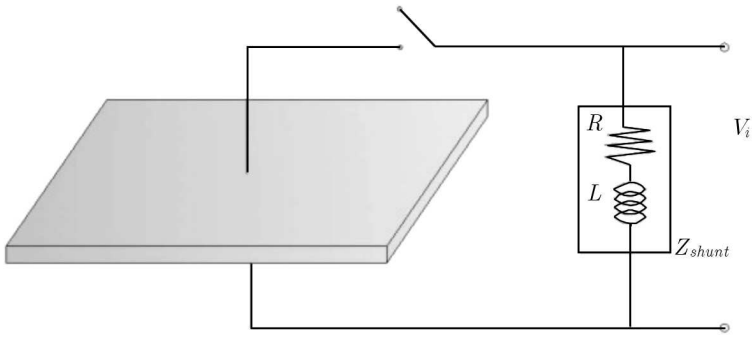

Fig. 2. Synchronised switched shunt circuit

A couple of collocated PZT patches are bonded to the structure. The idea is to generate the control force that opposes itself to the motion with the maximum amplitude and without tuning requirement. To this end, the "on" state (switch closed) is synchronised with the maximum signal detected by the sensors. This produces the maximum flowing charge into the inductor which sends it reversed to the actuator. This means that the control force is in phase opposition with respect to the local displacement of the structure.

Finally, the switching time, i.e. the period the circuit is switched on, is generally assumed 10 to 50 times lower than the mechanical period to control. The inductive element of the circuit is thus chosen according to Eq. (2.1), relating such an element to the piezo capacitance and the electric angular frequency (Clark, 1999, 2000; Ciminello *et al.*, 2008a,c; Corr and Clark, 2001, 2002, 2003; Corr, 2003; Hagood and van Flotow, 1991; Lesieutre, 1998; Richard *et al.*, 1999, 2000)

$$L = \frac{1}{\omega^2 C} \tag{2.1}$$

Moreover, if the switch mechanism is set according to the highest frequency of interest, the natural band range of the control system is naturally defined. To summarise circuit working modalities:

Open Circuit State: in absence of any shunted configuration, that is to say, no connection to a passive electrical network, no current flows and the voltage is a function of the displacement;

Shunted Circuit State: every time the piezo voltage reaches a maximum, the switch is closed. The connection of the PZT electrodes to the external circuit is realised. The voltage is given by two contributions: the open circuit signal (proportional to the deformations) added to the offset signal (proportional to the electrical charge).

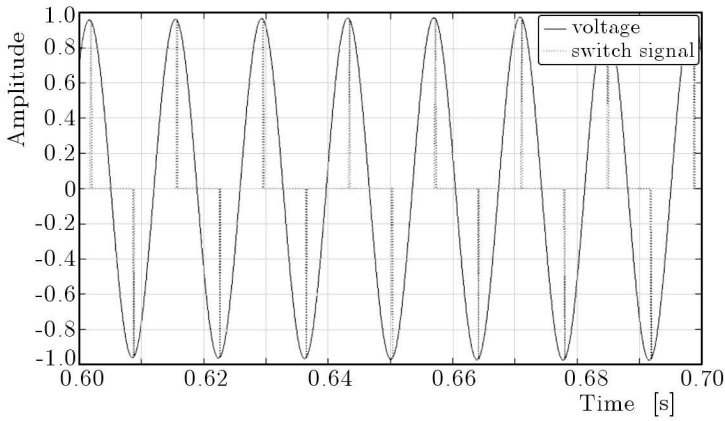

Fig. 3. Switch signal simulation

The switching mechanism produces naturally amplified voltage (Fig. 4) and the charge behaviour as shown in Fig. 5.

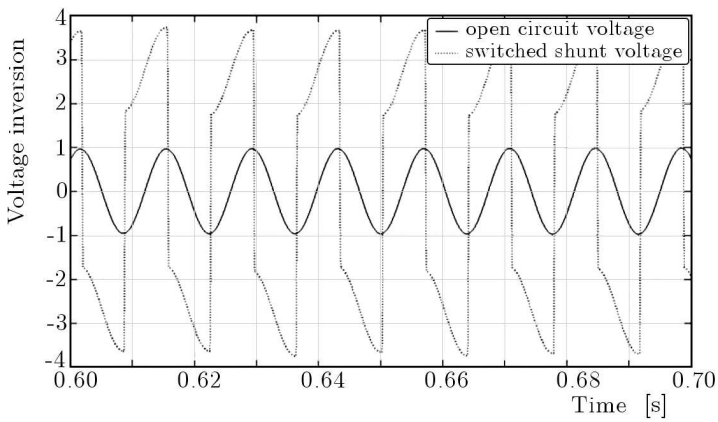

Fig. 4. Voltage signal simulation

The collocated configuration of the sensor-actuator and the absence of an external power supply, that means no energy injected into the system, guarantee unconditional stability of the control.

Some drawbacks can be found in the inner behaviour of the control. The effect of this kind of control is in fact the reduction of the vibration amplitude not by damping but subtracting a fraction of the mechanical energy of the system at resonance and giving it back, transferring energy to the high frequencies.

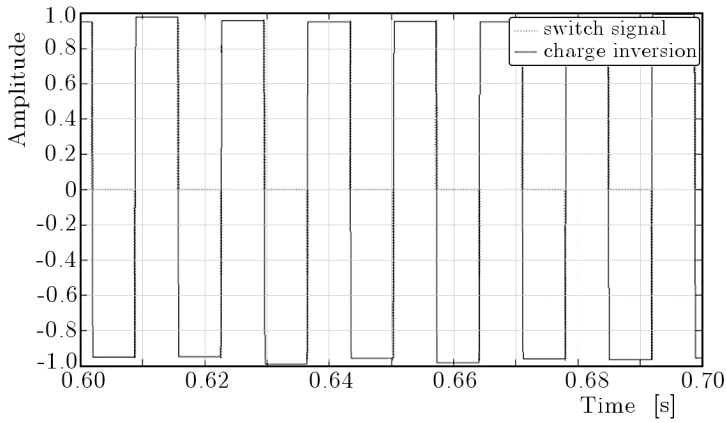

Fig. 5. Charge signal simulation

3. Problem formulation and solving strategy

The considered physical problem is sketched in Fig. 6. A 1D air column excited on the left boundary $(x = 0)$ by a signal $u_0(t)$

$$u_0(t) = U_0 \sin(\omega t) \qquad \forall t \tag{3.1}$$

and controlled on the right by two PZT patches bonded to an aluminium alloy plate (see detail at the bottom of Fig. 6).

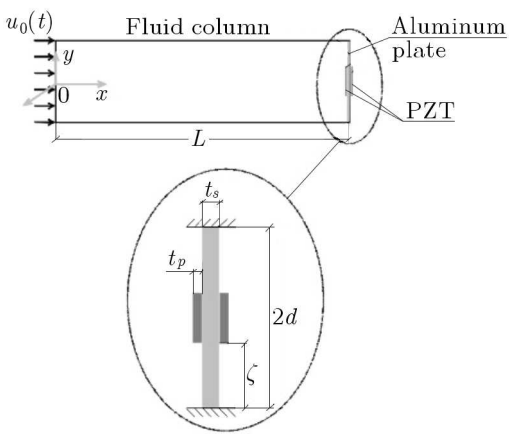

Fig. 6. Scheme of the problem

The displacement field $u(x,t)$ within the air column is described by the telegraph equation

$$\frac{\partial^2 u}{\partial t^2} - c^2 \frac{\partial^2 u}{\partial x^2} + \xi \frac{\partial u}{\partial t} = 0 \tag{3.2}$$

resulting from the application of the mass equation and the balance of inertial (time 2nd derivative), elastic (spatial 2nd derivative) and dissipative (time 1st derivative) forces, acting on a fluid element.

The boundary condition on the left side of the domain, coherently with (3.1), is given

$$u(0,t) = u_0(t) = U_0 \sin(\omega t) \qquad \forall t \tag{3.3}$$

The other boundary condition on the right side of the domain $(x = L)$ results from the formalisation of the fluid/structure interaction at the interface and from the semi-active nature of the switched shunt control. The structure, a plate very long in the z direction, behaves according to Timoshenko's "long rectangular plate" theory (Timoshenko and Woinowsky-Krieger, 1959).

The acoustic pressure at the interface, $p(L,t)$, jointly with the piezo action (moment $M_p(t)$), produces the displacement of the middle of the plate, $u_p(y=0)$, described by the classical elastic beam theory

$$u_p(t) = \frac{3}{8}\frac{p(L,t)b}{D} d^4 - \frac{M_p(t)}{D}\zeta\Big(\zeta - \frac{3}{2}\Big) d^2 \tag{3.4}$$

The same theory provides also the deformation within the piezo, ε_p. Then, by considering the piezoelectric constitutive law (Preumont, 1997), the open circuit voltage V can be computed

$$V = g_{31}\frac{E_p t_p}{1-\nu_p}\varepsilon_p \tag{3.5}$$

with b and D being the plate depth and bending stiffness, respectively.

This voltage, used by the logic to detect the instant at which the circuit must be switched on, is modified according to what was explained in the previous Section (Fig. 4, comparing the open state and circuit generated voltages).

By exploiting the Crawley and De Luis transmission model (Crawley and Luis, 1987) that proposes a linear relation between transmitted actions and applied voltage, the moment $M_p(t)$ can be computed.

Since the fluid and plate displacements are the same at the interface

$$u(L,t) = u_p(t) \qquad \forall t \tag{3.6}$$

and recalling that

$$p(x,t) = -\rho c^2 \frac{\partial u}{\partial x} \tag{3.7}$$

Eq. (3.4) can be finally rewritten to formalise the required boundary condition

$$\beta_1 \frac{\partial u}{\partial x}\bigg|_L + \beta_2 u(L,t) = E_0 \qquad \forall t \tag{3.8}$$

where

$$\beta_1 = 1 \qquad \beta_2 = \frac{8}{3}\frac{D}{\rho c^2 b d^4} \qquad E_0 = -\frac{8}{3}\frac{M_p(t)}{\rho c^2 b d^2}\zeta\Big(\zeta - \frac{3}{2}\Big) \tag{3.9}$$

For sake of simplicity, no inertial and damping terms have been taken into account in condition (3.8). This, as already mentioned, restricts the validity of the model to frequencies far from the structural resonance. Such an assumption is however coherent with the low band range of interest for the switched shunt control.

The initial conditions are represented by the displacement and velocity at the time t_0 described by the assigned functions $f(x)$ and $g(x)$

$$u(x,t) = f(x) \qquad \frac{\partial u}{\partial t}\bigg|_{t_0} = g(x) \qquad \forall x \tag{3.10}$$

To compute a semi-analytical solution, through a Fourier series expansion, boundary conditions (3.3) and (3.8) have to become homogeneous (Haberman, 1987). It is possible to demonstrate that this can be achieved by assuming the function

$$v(x,t) = u(x,t) + \Big(\frac{\beta_2 x}{\beta_1 + \beta_2 L} - 1\Big)U_0 \sin(\omega t) - \frac{E_0 x}{\beta_1 + \beta_2 L} \tag{3.11}$$

After introducing relation (3.11) into Eq. (3.2) and the related boundary conditions, (3.3) and (3.7), and initial conditions, (3.10), a new problem is found

$$\frac{\partial^2 v}{\partial t^2} - c^2 \frac{\partial^2 v}{\partial x^2} + \xi \frac{\partial v}{\partial t} = P(x,t) \tag{3.12}$$

Boundary conditions read

$$v(0,t) = 0 \qquad \beta_1 \frac{\partial v}{\partial x}\bigg|_L + \beta_2 v(L,t) = 0 \qquad \forall t \tag{3.13}$$

initial conditions read

$$v(x,t_0) = f(x) + Q(x,t_0) \qquad \frac{\partial v}{\partial t}\bigg|_{t_0} = g(x) + R(x,t_0) \qquad \forall x \tag{3.14}$$

where

$$
\begin{aligned}
P(x,t) &= U_0\omega\Big(\frac{\beta_2 x}{\beta_1+\beta_2 L}-1\Big)[\xi\cos(\omega t)-\omega\sin(\omega t)]\\
Q(x,t) &= \Big(\frac{\beta_2 x}{\beta_1+\beta_2 L}-1\Big)U_0\sin(\omega t)-\frac{E_0 x}{\beta_1+\beta_2 L}\\
R(x,t) &= U_0\omega\Big(\frac{\beta_2 x}{\beta_1+\beta_2 L}-1\Big)\cos(\omega t)
\end{aligned}
\tag{3.15}
$$

Equation (3.12) may be solved by separating space and time variables, i.e. assuming the solution $v(x,t)$ as a product of the two unknown functions, X and T, the former depending on x, the latter on t

$$
v(x,t) = X(x)T(t) \tag{3.16}
$$

As a result, Eq. (3.12) is split into two separated problems

$$
\frac{d^2X}{dx^2}+\lambda^2 X(x)=0 \qquad\qquad \frac{d^2T}{dt^2}+\xi\frac{dT}{dt}+c^2\lambda^2 T(t)=0 \tag{3.17}
$$

The solution to $(3.17)_1$ can be expressed as a sum of infinite orthogonal functions, $\varphi_n(x)$, satisfying conditions (3.13)

$$
\varphi_n(x)=\sin(\lambda_n x) \tag{3.18}
$$

being λ_n the nth root of the transcendental eqauation (Boyce and DiPrima, 2008)

$$
\beta_1\lambda_n+\beta_2\tan(\lambda_n L)=0 \tag{3.19}
$$

By expressing the solution $v(x,t)$ as a sum of the products of these functions with the corresponding time dependent ones, $b_n(t)$

$$
v(x,t)=\sum_{n=1}^{\infty}\varphi_n(x)b_n(t) \tag{3.20}
$$

Eq. $(3.10)_2$ can be written into a new formalism

$$
\sum_{n=1}^{\infty}\varphi_n(x)\Big(\frac{d^2b_n}{dt^2}+\xi\frac{db_n}{dt}+c^2\lambda_n^2 b_n(t)\Big)=P(x,t) \tag{3.21}
$$

This relation, by introducing the Fourier expansion of $P(x,t)$

$$
P(x,t)=\sum_{n=1}^{\infty}\varphi_n(x)p_n(t) \tag{3.22}
$$

with

$$p_n(t) = \frac{\int_0^L P(x,t)\varphi_n(x)\,dx}{\int_0^L \varphi_n^2(x)\,dx} = \frac{2U_0\omega[\xi\cos(\omega t) - \omega\sin(\omega t)]}{[\cos(\lambda_n L)\sin(\lambda_n L) - \lambda_n L]} \tag{3.23}$$

reduces itself to a time dependent equation

$$\frac{d^2 b_n}{dt^2} + \xi\frac{db_n}{dt} + c^2\lambda_n^2 b_n(t) = p_n(t) \tag{3.24}$$

Equation (3.24) assumes the solution in the form

$$b_n(t) = \underbrace{[D_{1n}\sin(\omega_n t) + D_{2n}\cos(\omega_n t)]\mathrm{e}^{-\frac{1}{2}\xi t}}_{\text{general integral}} + \underbrace{A_n\sin(\omega t) + B_n\cos(\omega t)}_{\text{particular integral}} \tag{3.25}$$

with

$$\omega_n = \sqrt{c^2\lambda_n^2 - \frac{\xi^2}{4}} \tag{3.26}$$

The constants A_n and B_n can be determined by substituting the particular integral into Eq. (3.24)

$$\begin{aligned} A_n &= 2U_0\omega^2\frac{\xi^2 - (c^2\lambda_n^2 - \omega^2)}{[\xi^2\omega^2 + (c^2\lambda_n^2 - \omega^2)^2][\cos(\lambda_n L)\sin(\lambda_n L) - \lambda_n L]} \\ B_n &= 2U_0\omega\xi\frac{c^2\lambda_n^2}{[\xi^2\omega^2 + (c^2\lambda_n^2 - \omega^2)^2][\cos(\lambda_n L)\sin(\lambda_n L) - \lambda_n L]} \end{aligned} \tag{3.27}$$

The remaining constants, D_{1n} and D_{2n}, can be computed by imposing that $v(x,t)$, formalised as in (3.20) and including (3.25), satisfies initial conditions (3.14):
— 1st initial condition

$$D_{1n}\sin(\omega_n t_0) + D_{2n}\cos(\omega_n t_0) = [-A_n\sin(\omega t_0) - B_n\cos(\omega t_0) + \mu_n + q_n(t_0)]\mathrm{e}^{\frac{\xi}{2}t_0} \tag{3.28}$$

— 2nd initial condition

$$\begin{aligned} &D_{1n}\Big[\omega_n\cos(\omega_n t_0) - \frac{\xi}{2}\sin(\omega_n t_0)\Big] - D_{2n}\Big[\omega_n\sin(\omega_n t_0) + \frac{\xi}{2}\cos(\omega_n t_0)\Big] = \\ &\quad = [-A_n\omega\cos(\omega t_0) + B_n\omega\sin(\omega t_0) + \nu_n + r_n(t_0)]\mathrm{e}^{\frac{\xi}{2}t_0} \end{aligned} \tag{3.29}$$

being μ_n, ν_n, q_n and r_n the terms of the Fourier series expansion of $f(x)$, $g(x)$, $Q(x,t)$ and $R(x,t)$, respectively

$$\mu_n = \frac{\int_0^L f(x)\varphi_n(x)\,dx}{\int_0^L \varphi_n^2(x)}\,dx \qquad \nu_n = \frac{\int_0^L g(x)\varphi_n(x)\,dx}{\int_0^L \varphi_n^2(x)\,dx}$$

$$q_n(t) = \frac{\int_0^L Q(x,t)\varphi_n(x)\,dx}{\int_0^L \varphi_n^2(x)\,dx} = \frac{2E_0}{\lambda_n(\beta_1+\beta_2 L)} - \frac{2U_0\sin(\omega t)}{\lambda_n L - \sin(\lambda_n L)\cos(\lambda_n L)} \tag{3.30}$$

$$r_n(t) = \frac{\int_0^L R(x,t)\varphi_n(x)\,dx}{\int_0^L \varphi_n^2(x)\,dx} = -\frac{2U_0\cos(\omega t)}{\lambda_n L - \sin(\lambda_n L)\cos(\lambda_n L)}$$

Finally, by assembling (3.11), (3.18), (3.20) and (3.25), the required solution to problem (3.2) can be written

$$u(x,t) = \sum_{n=1}^{\infty} \sin(\lambda_n x)\{[D_{1n}\sin(\omega_n t) + D_{2n}\cos(\omega_n t)]\mathrm{e}^{-\frac{\xi}{2}t} + \\ + A_n\sin(\omega t) + B_n\cos(\omega t)\} - \Big(\frac{\beta_2 x}{\beta_1+\beta_2 L} - 1\Big)U_0\sin(\omega t) + \frac{E_0 x}{\beta_1+\beta_2 L} \tag{3.31}$$

The corresponding pressure field, $p(x,t)$, may be obtained by deriving with respect to x the above solution and multiplying it by $-\rho c^2$

$$p(x,t) = -\frac{1}{\rho c^2}\sum_{n=1}^{\infty} \lambda_n\cos(\lambda_n x)\{[D_{1n}\sin(\omega_n t) + D_{2n}\cos(\omega_n t)]\mathrm{e}^{-\frac{\xi}{2}t} + \\ + A_n\sin(\omega t) + B_n\cos(\omega t)\} - \frac{\beta_2 U_0\sin(\omega t) + E_0}{\beta_1+\beta_2 L} \tag{3.32}$$

The corresponding pressure squared value averaged with respect to space and time has been computed

$$\widehat{p} = \frac{1}{T_{tot}}\int_{t_0}^{t_0+T_{tot}} \frac{1}{L}\int_0^L p^2(x,t)\,dx\,dt \tag{3.33}$$

For the no control case, simulation relations (3.31) and (3.32) can be exploited to compute the displacement and pressure field within the entire considered time interval. On the other hand, for the switched control simulation, due to the discontinuity of circuit parameters, like voltage, charge and hence E_0, the use of (3.31) and (3.32) is restricted to the time intervals in which the circuit parameters keep constant, that is during the switch on and off stationary states. In practice, the solution at any time interval is computed by assuming as initial conditions the configuration (in terms of displacement and velocity) computed at the last instant of the previous time interval.

4. Numerical results

The results herein presented have been obtained considering the parameters summarised in Table 1.

Before computing the displacement field (in Fig. 14) and corresponding pressure distribution, a preliminary validation process has been carried out on solution (3.31).

At first, the validation of boundary conditions (3.3) and (3.7) has been proved, just expressing relation (3.28) at $x = 0$ and $x = L$. Then, the convergence of coefficients A_n, B_n, D_{1n}, D_{2n} has been verified by exciting the system far and at the fluid resonance. In Figs. 7-9, the mentioned coefficients vs. harmonic order n have been plotted at 50 Hz and for the first two normal modes.

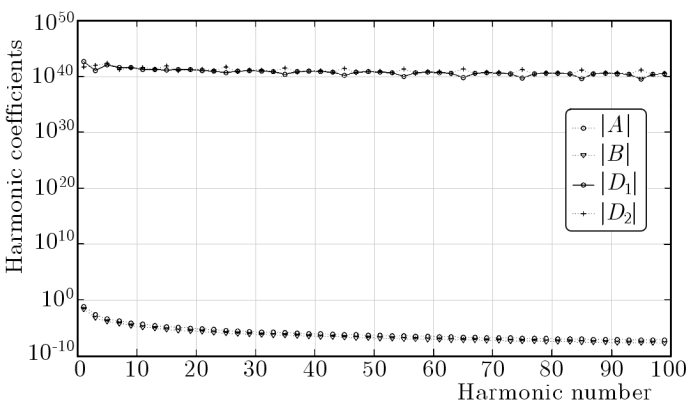

Fig. 7. Fourier series coefficients vs. harmonic order at an excitation frequency of 50 Hz

Table 1. Simulation parameters

Main simulation parameters	
Time interval	
1st resonance frequency [Hz]	170
2nd resonance frequency [Hz]	340
Frequency considered for out of resonance simulations [Hz]	50
Fluid column properties	
Length [m], L	1
Depth [m], b	0.5
Height [m], $2d$	0.06
Density [kg/m^3], ρ	1.19
Sound speed [m/s], c	340
Decay rate [dB/s], ξ [28]	200
Beam properties	
In-plane (yz) dimensions [m]	0.06×0.5
Thickness [m], t_s	$5 \cdot 10^{-4}$
Young modulus [GPa], Y_s	72
Poisson ratio, ν_s	0.33
Density [kg/m^3], ρ_s	2700
1st resonance frequency [Hz], f_s	737
Piezo properties	
In-plane (yz) dimensions [m]	0.03×0.5
Thickness [m], t_p	$5 \cdot 10^{-4}$
Young modulus [GPa], Y_p	59
Poisson ratio, ν_p	0.32
d_{31} [m/V]	$-35 \cdot 10^{-11}$
g_{31} [Vm/N]	$8 \cdot 10^{-3}$

The evident convergence allows for considering a small order for a good solution accuracy.

After this preliminary validation, the results in terms of the displacement and sound pressure level have been computed in the time domain. At first, the lowest resonance frequency of the structure has been estimated and assumed as the upper threshold, coherently with the assumption boundary conditions (3.7) based on the absence of structural inertial and damping actions.

The normalised displacement vs. time and column axis, at 50 Hz and for the first two resonance frequencies without control has been plotted in Figs. 10-12.

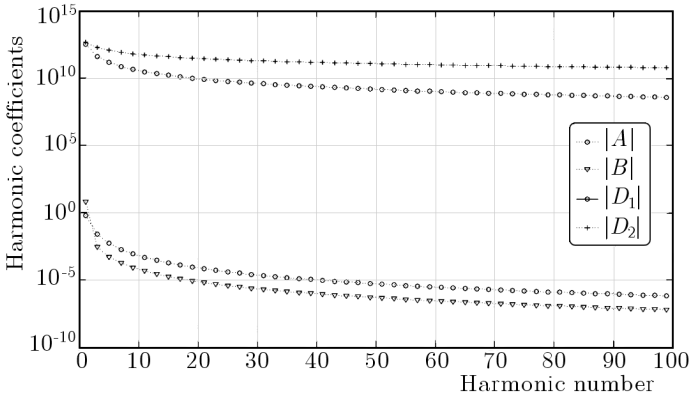

Fig. 8. Fourier series coefficients vs. harmonic order at the 1st resonance frequency

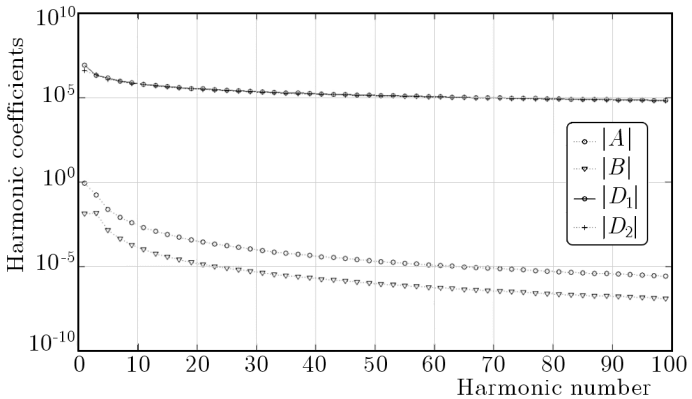

Fig. 9. Fourier series coefficients vs. harmonic order at the 2nd resonance frequency

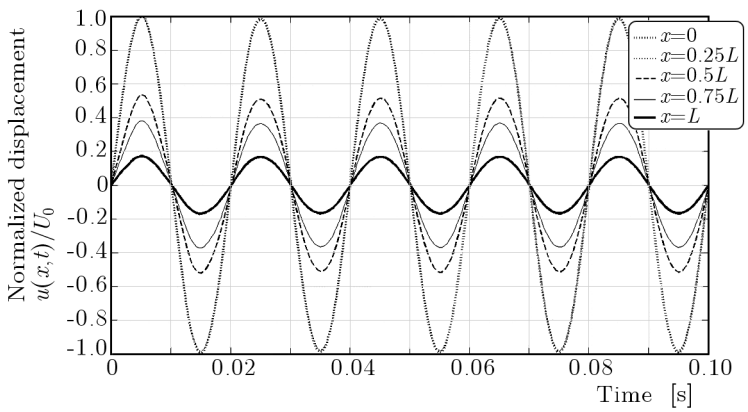

Fig. 10. Normalised displacement vs. time for $x/L = 0$, 0.25, 0.50, 0.75, 1 at 50 Hz

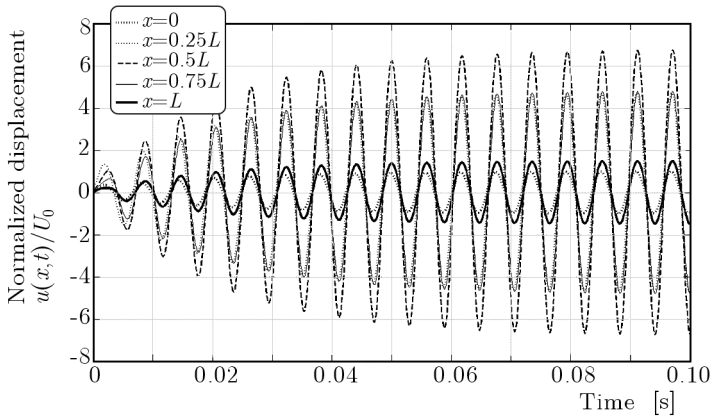

Fig. 11. Normalised displacement vs. time for $x/L = 0$, 0.25, 0.50, 0.75, 1 at the 1st resonance frequency

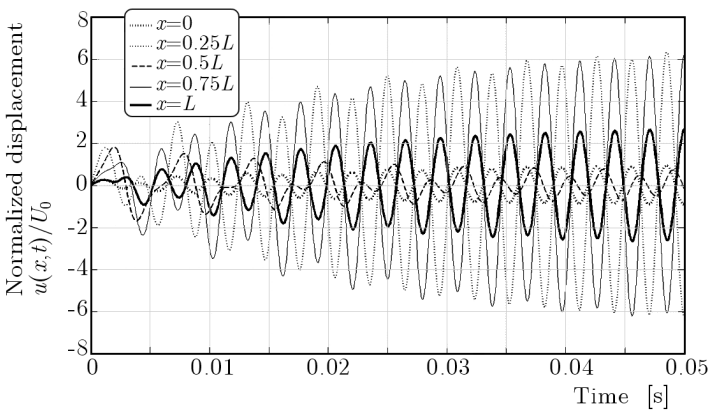

Fig. 12. Normalised displacement vs. time for $x/L = 0$, 0.25, 0.50, 0.75, 1 at the 2nd resonance frequency

The corresponding modal shapes of the fluid column have been extracted at a fixed time in the steady state regime, from the last two figures (see Fig. 13).

The normalised displacement at $x = L$ vs. time, for the first two resonance frequencies and gain amplification of 1 and 10 have been compared with no controlled response in Figs. 14 and 15.

In Fig. 14, one can easily see the circuit ability of inducing also a phase shift (Petit *et al.*, 2002, 2004; Richard *et al.*, 1999, 2000).

Finally, in Figs. 16 and 17, the normalised displacement field and the difference between no controlled and controlled (amplification = 1) case vs. time and column axis have been plotted.

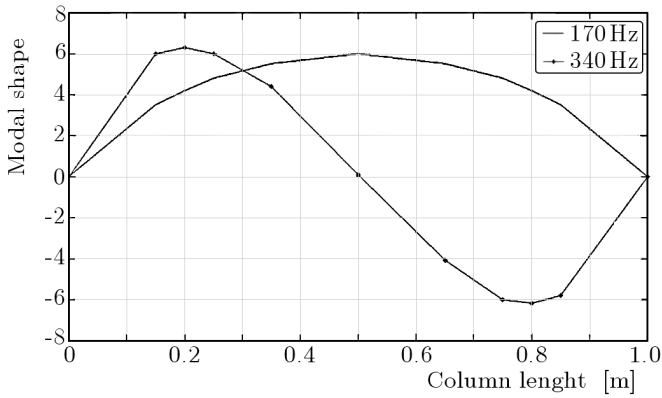

Fig. 13. 1st and 2nd modal shapes

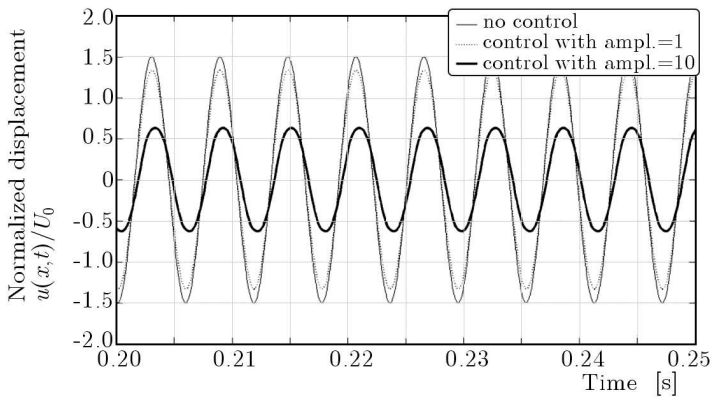

Fig. 14. Normalised displacement vs. time and amplification level at $x = L$ for the first resonance

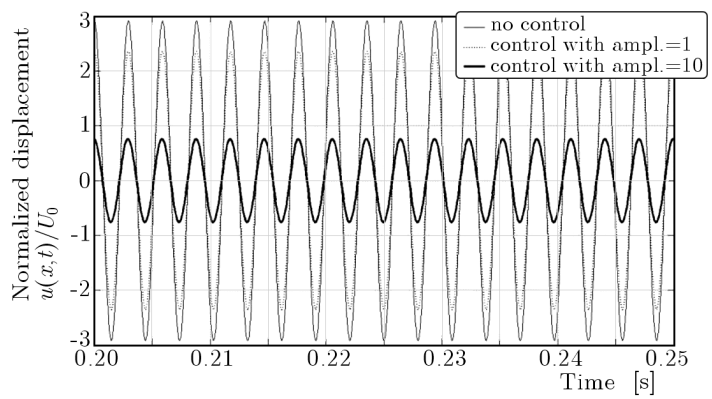

Fig. 15. Normalised displacement vs. time and amplification level at $x = L$ for the second resonance

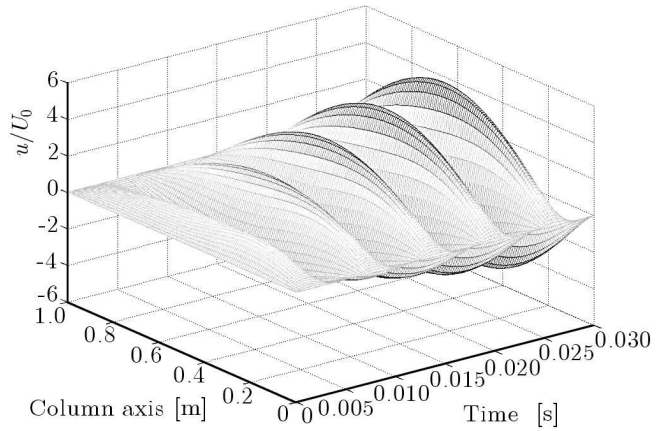

Fig. 16. Normalised displacement vs. time and column axis for the first resonance

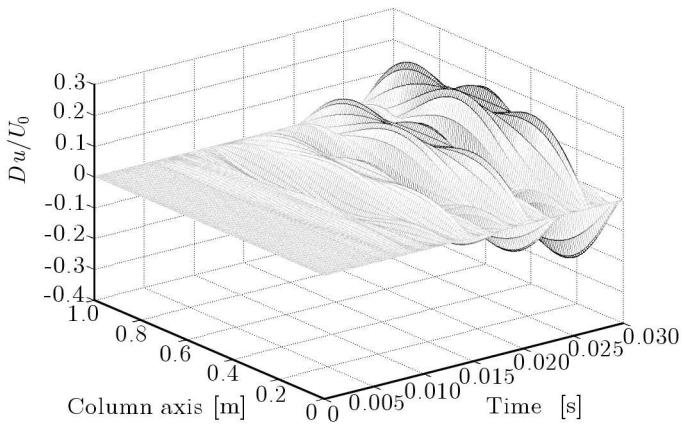

Fig. 17. No controlled-controlled normalised displacement difference vs. time and column axis for the first resonance

An attenuation of 1.5 and 2.3 dB without amplification has been estimated at the fluid-structure interface for the first and second resonance frequencies. The maximum reduction (7.9, 11.2 dB at 170 and 340 Hz, respectively) has been observed for the maximum amplification considered.

To have an idea of the energy attenuation, the squared value of the pressure has been computed and reported for fixed locations along the column. The corresponding squared mean energy, SME, estimated through (3.33), has been reported on the last column.

Benefits are evident for different locations along the fluid column, even though zero attenuation values have been detected on the modal shape nodes.

Table 2. Sound pressure reduction vs. spatial domain and amplification

First resonance: 170 Hz						
x/L / Gain	0	0.25	0.50	0.75	1.00	SME
	Sound pressure attenuation [dB]					
1	2.1	1.9	0	1.8	1.5	1.7
5	5.7	5.1	0	5.1	5.4	9.7
10	12	10	0	9.8	9.5	17.3
Second resonance: 340 Hz						
x/L / Gain	0	0.25	0.50	0.75	1.00	SME
	Sound pressure attenuation [dB]					
1	2.8	0	2.3	0	2.1	3.8
5	8.5	0	8.3	0	8.2	15.2
10	13	0	14	0	14	24.6

Generally, the control proved to be more effective for the 2nd frequency, by achieving a mean reduction of 24.6 dB, 6.5 times higher than in the reference case without amplification. The minimum averaged attenuation (1.7 dB) has been detected for the 1st resonance, without amplification.

Finally, to have an idea of control authority for the entire frequency range (0-500 Hz), the mean pressure level estimated with and without control (for Gain = 1) by exciting the system through a stepped sine signal has been compared in Fig. 18.

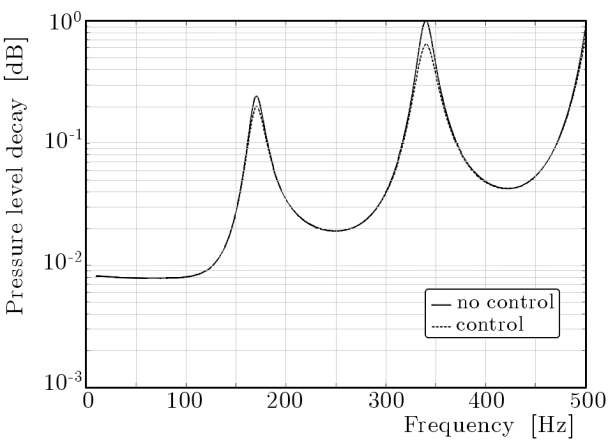

Fig. 18. No controlled-controlled mean pressure level vs. frequency

The related attenuation, as shown in Fig. 19, has proved to mainly interest the peaks zones.

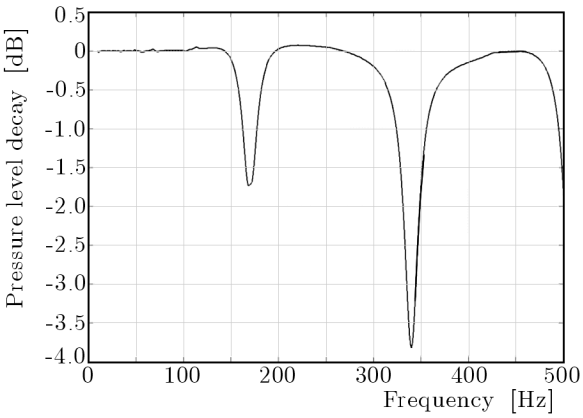

Fig. 19. No controlled-controlled dB mean pressure level reduction vs. frequency

5. Conclusions and further steps

In the present work, the possibility of exploiting the switched shunt control architecture to sound pressure attenuation within enclosures has been dealt with. Many applications have been already published on the vibration attenuation through piezo network controlled by this mentioned logic. The related benefits within the low frequency band led to development of numerical tools aimed at predicting related benefits, and addressing experimental campaigns to verify effectiveness and point out eventual drawbacks.

Also, applications focused on acoustic problems have been carried out, generally oriented to interior noise radiation and sound pressure level within enclosures.

The main advantage of the switch logic is fully described in the referred literature and summarised in the dedicated Sectio of the present paper. The idea is to generate a control force opportunely synchronised to the maximum amplitude and shortly temporised with the sensor output signal. These operating conditions guarantee a pulse kind actuation force out of phase with respect to the local structural displacement and independent of the structural response in a wide band range.

Moreover, being the resistor negligible, the switched shunt performs more thermal stability.

The absence of an external power supply injecting energy into the system guarantees an unconditional stability of the control.

The paper at hand is concerned with the formalisation of a semi-analytical solution describing the displacement and pressure field within an air column

subjected to switch control, implemented to a piezo actuator. This approach ensures quick estimation of the efficiency of the control acting within an enclosure, exploitable as the preliminary design reference for further, more complex, numerical modelling.

The acoustic field is described by the telegraph equation whose solution has been expressed as a Fourier expansion. The disturbance (sinusoidal excitation) and control action (given by a long plate actuated by a piezo) have been supposed localised on two boundaries of a 1D domain.

At first, a preliminary validation of the solution has been addressed, tracking series coefficients vs. harmonic order behaviour. Secondly, modal shapes have been plotted for the first two resonances without control. Then the control authority has been investigated, computing the displacement vs. time as well as vs. amplification gain at fixed locations along the column axis. The related information has been expressed in terms of the punctual and averaged sound pressure level. Larger authority has been observed for the 2nd normal frequency: 24.6 dB of attenuation, with a 10-times amplification. Even without any amplification, coherently with the semi-passive nature of this control, a reduction of 3.8 dB has been estimated.

In order to assess the model validity and to point out possible limits, a tailored experimental prototype; more in detail – a duct instrumented with microphones along the generatrix with a loudspeaker and a pzt controlled panel mounted on the bases, will be manufactured.

The above mentioned model can be further enriched by introducing impedance for damping layer applications. Moreover, the solution validity can be extended in the frequency band, even though paying in terms of complexity, introducing the effects of structural inertial and damping actions.

Finally, different and more complex geometries, of major interest for real applications (axial-symmetric, tapered, etc), could be investigated by formalising the problem through tailored boundary conditions.

References

1. Ameduri S., Ciminello M., Concilio A., 2007, Semi-analytical solution of a structural system controlled by a switched shunt architecture, *Proceeding of the 36th International Congress and Exhibition on Noise Control Engineering – Session ANVC "Active Noise and Vibration Control"*, Istanbul, Turchia, Paper IN07-032

2. Boyce W.E., DiPrima R.C., 2008, *Elementary Differential Equations and Boundary Value Problems*, Jhon Wiley & Sons Inc, seventh edition, 621-655

3. Ciminello M., Ameduri S., Calabrò A., Concilio A., 2008a, Synchronised switched shunt control technique applied on a cantilevered beam: numerical and experimental investigations, *JIMSS*, **19**, 9, 1089-1100

4. Ciminello M., Deu J.-F., Ohayon R., Ameduri S., 2008b, Vibration reduction of structural-acoustic systems using synchronized switch damping techniques, *Proceeding of 2008 ASME International Conference on Smart Materials, Adaptive Structures and Intelligent Systems*, Ellicot City, MD, USA, Paper SMASIS08-320

5. Ciminello M., Lecce L., Ameduri S., Calabrò A., Concilio A., 2008c, Switched shunt control implemented through a PZT network embedded within a composite panel: design, manufacture and test, submitted to *JIMSS-08-452*

6. Clark W., 1999, State switched piezoelectric systems for vibration control, *Structure, Structural Dynamics and Materials AIAA Journal*, **1533**, 2623-2629

7. Clark W., 2000, Vibration control with state-switched piezoelectric materials, *Journl of Intelligent Material Systems and Structures*, **11**, 263-273

8. Collinger J.C., Wickert J.A., 2007, Adaptive piezoelectric vibration control with synchronized swtching, *Porceeding of ASME International Mechanical Engineering Congress and Exposition, IMECE 2007-41427*, Seattle, Washington, USA

9. Corr L.R., 2001, Investigation of real-time switching of piezoceramic shunts for structural vibration control, *PhD Thesis*, School of Engineering, University of Pittsburg

10. Corr L., Clark W., 2001, Energy dissipation of piezoelectric semi-active vibration control, *Journal of Intelligent Material Systems and Structures*, **12**, 729-736

11. Corr L., Clark W., 2002, Comparison of low-frequency piezoelectric switching shunt technique for structural damping, *Smart Materials and Structures*, **11**, 370-376

12. Corr L., Clark W., 2003, A novel semi-active multimodal vibration control law for a piezoceramic actuator, *Journal of Vibration and Acoustics*, **125**, 214-222

13. Crawley E.F., de Luis J., 1987, Use of piezoelectric actuators as elements of intelligent structures, *AIAA Journal*, **25**, 10, 1373-1385

14. De Marneffe B., Horodinca M., Preumont A., 2008, Vibration isolation via shunted electromagnetic transducer, *Proceedings of ISMA2008*, Leuven, Belgium, isma2008-0499

15. DUCARNE J., THOMAS O., DEU J.-F., 2007, Structural vibration reduction optimization by switch shunting of piezoelectric elements, *Proceeding of ASME International Mechanical Engineering Congress and Exposition, IMECE 2007-41427*, Seattle, Washington, USA

16. ERTURK A., INMAN D.J., 2008, Piezoelectric shunt damping for chatter suppression in machining processes, *Proceedings of ISMA2008*, Leuven, Belgium, isma2008-0296

17. EVEREST F.A., 2001, *The Master Handbook of Acoustics*, Mc Graw-Hill International Editions, fourth edition, 142-147

18. GUYOMAR D., BADEL A., 2006, Nonlinear semi-passive multimodal vibration damping: an efficient probabilistic approach, *Journal of Sound and Vibration*, **294**, 249-268

19. HABERMAN R., 1987, *Elementary Applied Partial Differential Equations with Fourier Series and Boundary Value Problems*, Prentice Hall Inc., second edition, 257-261

20. HAGOOD N.W., VON FLOTOW A., 1991, Damping of structural vibrations with piezoelectric materials and passive electrical networks, *MIT Journal of Sound and Vibration*, **146**, 2, 243-268

21. LALLART M., BADEL A., GUYOMAR D., LEBRUN L., 2005, Non-linear semi-passive damping using constant or adaptive voltage source: a stability analysis, *ICAST 2005 – 16th International Conference on Adaptive Structures and Technologies*, 158-165

22. LEFEUVRE E., BADEL A., PETIT L., RICHARD C., GUYOMAR D., 2006, Semi-passive piezoelectric structural damping by synchronized switching on voltage source, *Journal of Intelligent Material Systems and Structures*, **17**, 653-660

23. LESIEUTRE G.A., 1998, Vibration damping and control using shunted piezoelectric materials, *The Shock and Vibration Digest*, **30**, 3, 187-195

24. PARK G., INMAN D.J., 1999, A uniform model for series RL and parallel RL shunt circuits and power consumption, *SPIE Conference Proceedings on Smart Structure and Integrated Systems*, Newport Beach, CA, 3668, 797-804

25. PETIT L., GUYOMAR D., RICHARD C., 2002, Piezoelectric damping: a comparison between passive and semipassive switching techniques, *Proc. of 4th JFSIMS – Japan-France Seminar on Intelligent materials and Structures*, Lyon

26. PETIT L., LEFEUVRE E., RICHARD C., GUYOMAR D., 2004, A broadband semi passive piezoelectric technique for structural damping, *Proc. of SPIE*, **5386**, 414-425

27. PREUMONT A., 1997, *Vibration Control of Active Structures: An Introduction*, Kluwer Academic Publishers

28. Richard C., Guyomar D., Audigier D., Bassaler H., 2000, Enhanced semi-passive damping using continuous switching and Isolation, *SPIE*, **3989**, 288-299

29. Richard C., Guyomar D., Audigier D., Ching G., 1999, Semi-passive damping using continuous switching of a piezoelectric device, *Society of Photo-Optical Instrumentation Engineering (SPIE) Conference Series*, **3672**, 104-111

30. Timoshenko S.P., Woinowsky-Krieger S., 1959, *Theory of Plates and Shells*, Mc Graw-Hill International Editions, second edition, 4-6

Rozwiązanie Fouriera dla przewodu akustycznego z bocznikującym układem sterowania

Streszczenie

W pracy zaprezentowano pół-analityczne rozwiązanie zagadnienia redukcji poziomu ciśnienia akustycznego w przewodzie za pomocą zsynchronizowanej metody bocznikowania. Opis pola przemieszczeń wewnątrz jednowymiarowej kolumny powietrza sformalizowano rozwinięciem w szereg Fouriera przy uwzględnieniu sinusoidalnie zmiennych zaburzeń na prawym i lewym brzegu przewodu. Dla przypadku z wyłączonym układem sterowania rozwiązanie obliczono w całej dziedzinie czasu przy utrzymaniu stałych parametrów obwodu elektrycznego, natomiast dla trybu sterowanego dokonano analizy, dzieląc przedział czasu na fragmenty. W każdym z nich charakterystyczne cechy układu sterowania (np. napięcie przykładane do piezoelektryków, natężenie pola elektrycznego...) dobrano w odpowiedni sposób. Na podstawie obserwacji przemieszczeń porównano poziom ciśnienia akustycznego dla warunków z wyłączonym i włączonym sterowaniem oraz z i bez wzmocnienia sygnału.

Manuscript received July 6, 2009; accepted for print November 16, 2009